SSM/I Sea Ice Remote Sensing for Mesoscale Ocean-Atmosphere Interaction Analysis

Lars Kaleschke, Georg Heygster
Institute of Environmental Physics, University Bremen, Bremen
P.O. Box 33 04 40, D-28334 Bremen, Germany,
Phone: +49(0)421 218-4726, FAX: -4555, e-mail:lars@seaice.de,
http://www.seaice.de,http://www.iup.physik.uni-bremen.de/

Christof Lüpkes, Axel Bochert, Jörg Hartmann
Alfred Wegener Institute for Polar and Marine Research, Bremerhaven, Germany

Jörg Haarpaintner
Norwegian Polar Institute, Polarmiljosenteret, N-9296 Tromso, Norway

Timo Vihma
Finnish Institute of Marine Research, Helsinki, Finland

Published in the Canadian Journal of Remote Sensing
Focus Issue on Ice and Icebergs, October 2001

Abstract

Two algorithms have been used in a hybrid scheme in order to obtain sea ice concentration maps at 12 km resolution from Special Sensor Microwave Imager (SSM/I) data. One algorithm is based on the 85 GHz polarization difference. The second algorithm is the NASA Team algorithm using the 19 and 37 GHz SSM/I channels.

Using 85 GHz SSM/I data allows a significant resolution improvement compared to 19 GHz SSM/I data. This, however, requires to carefully consider the larger atmospheric opacity affecting SSM/I measurements at 85 GHz (weather influence) which can lead to incorrect sea ice concentration estimates - particularly over open water.

Our scheme combines the high spatial resolution achieved with the 85 GHz channels with the almost weather-independently NTA-based decision whether the data points belong to the ice-free ocean or to the ice-covered area.

Reference 85 GHz brightness temperatures (tie points) have been estimated using a statistical linear regression method with the aid of independent sea ice concentration reference data. These were derived from aircraft dual-polarized passive microwave measurements at 19 and 37 GHz and optical line scanner images.

The evaluation of 30 days of SSM/I data comparing the NTA and 85 GHz ice concentrations indicates a good agreement and a strong linear relationship.

ERS-2 SAR and SSM/I data were used to analyse the evolution of the Storfjorden Polynya and the MIZ in the Fram Strait. Two different numerical atmospheric models were used to analyse the effect of a resolution improvement from 50 to 12 km of the sea ice concentration data prescribed to model the atmospheric boundary layer (ABL). It was found that the representation of the MIZ substantially influences the modelled ABL temperatures. Temperature profiles obtained with the model using the high resolution sea ice concentration data agree significantly better with the profiles measured by the aircraft.

1 Introduction

For about thirty years microwave remote sensing techniques have been used for sea ice observations. Advances in satellite sensor technology have led to a considerable improvement of spatial resolution and accuracy of the measured quantities.

Maps showing the percentage area coverage of water with sea ice (sea ice concentration) are useful for ship navigation as well as for use in models of the Earth's climate system and the regional weather. The spatial resolution of these numerical models describing different components of the Earth's climate system, the ocean, atmosphere, and cryosphere, continues to increase.

Regional high resolution atmospheric models runs operational with a few km and down to some 100 m resolution. Process studies have been carried out with mesoscale models in polar regions at horizontal resolutions of 4 km and less (e.g. Vihma, 1995; Birnbaum and Lüpkes, submitted). The heat and momentum fluxes at the boundary of atmosphere and ocean significantly depend on the ice concentration (Ledley, 1988).

This is especially true during winter when the temperature difference between near-surface cold air and the surface of open water within the Arctic pack ice or in the marginal sea ice zone (MIZ) can reach 40 K. Under such conditions strong ice production occurs (Cavalieri and Martin, 1994). During the ice formation two thirds of the initial water salinity are being released as brine (Martin and Kauffman, 1981). Because the released brine is denser than the surrounding water masses, it sinks and induces convection in the ocean (Aagaard and Carmack, 1989).

This paper is based on results of the Arctic Radiation and Turbulence Interaction STudy (ARTIST), which was conducted in the environment of the Svalbard archipelago in March and April 1998. The core activity of the ARTIST project was an extensive field study with ground based and airborne measurements accompanied by adequate model experiments. A comprehensive description of the ARTIST work can be found in Hartmann *et al.* (1999) or at the ARTIST website (`http://www.awi-bremerhaven.de/ATM/ARTIST/`). The section of the Storfjorden Polynya was a result of independent work, which was not part of the ARTIST project.

The goal of our study is to develop an improved method for the production of sea ice concentration maps with 12 km resolution derived from satellite passive microwave data and to demonstrate the benefits of a higher spatial resolution for modelling the atmospheric boundary layer.

We first outline the relevant data sources, the ARTIST aircraft measurements, and the satellite observations from the Special Sensor Microwave Imager (SSM/I) and the synthetic aperture radar on board the second European Remote Sensing Satellite (ERS-2 SAR).

Then we present a framework for the fusion of sea ice concentration data from two different SSM/I algorithms, the NASA Team algorithm and Svendsen's *et al.* (1987) model applied to the 85 GHz SSM/I data.

We provide in the first place a method to derive reference brightness temperatures (tie points) for sea ice and open water which can be used with Svendsen's near 90 GHz algorithm. Secondly we combine the 85 GHz SSM/I channels with the other SSM/I channels in order to reduce atmospheric effects. The tie points are derived using aircraft data and they are used to calculate ice concentrations. After that we compare the results to those of the NASA Team algorithm, which was applied to aircraft as well as satellite data. Next we interprete the SSM/I ice concentration data using ERS-2 SAR images. Finally the results serve to investigate the sensitivity of atmospheric models to the sea ice concentration.

2 Data set

During ARTIST several satellite under-flights were carried out with the research aircraft Polar 2 and Polar 4 of the Alfred Wegener Institute for Polar and Marine Research (AWI) while operating equipment for remote sensing. This equipment consists of microwave radiometers, line scanners, radiation thermometer, and a laser altimeter, as well as several sensors for measuring meteorological parameters. The non-imaging dual-polarized 19 and 37 GHz radiometers mounted on Polar 4 allow to scan the surface below the aircraft at an incidence angle of 53° similar to the viewing geometry of the SSM/I. The cross-track line scanner measures the solar radiation reflected by the ground surface (Bochert, 1999). The aircraft in-situ measurements (air temperature, humidity, pressure, wind) are used in the modelling studies to assess the effect of the improved spatial resolution of the ice cover on the development of the atmospheric boundary layer.

The SSM/I sensor is an imaging microwave radiometer. It has been launched as part of the Defense Meteorological Satellite Program (DMSP) on the series of DMSP F-x satellites. The SSM/I measures dual-polarized microwave radiances at 19, 37 and 85 GHz and vertically polarized radiances at 22 GHz. The SSM/I scans the Earth's surface conically with a swath of 1400 km width. Thus the SSM/I, operating from a near-polar orbit, provides an almost global coverage every day. The sampling distance is 12.5 km at the 85 GHz channels and 25 km at the other channels. The spatial resolution depends on the frequency (Table 1) because the SSM/I utilizes only one broadband antenna and the spatial resolution is determined by diffraction.

The ERS-2 SAR gains surface information in very high spatial resolution of about 25 m, within a 100 km wide swath and with limited temporal access. The ERS-2 SAR operates at a frequency of 5.3 GHz (C-band) at an incidence angle of about 23° with VV-polarization (vertical on transmit, vertical on receive) (Kramer, 1996). For ARTIST, we acquired 40 ERS-2 SAR images partly coincident with the aircraft flights.

3 SSM/I algorithms

Several algorithms exist to derive the sea ice concentration from SSM/I data. The differences between the techniques consist in a different choice and utilization of the sensor channels, and in different tie points.

The NASA Team algorithm (NTA) is widely used and was therefore selected as a reference in this study (Cavalieri *et al.*, 1984; Cavalieri *et al.* 1991).

It makes use of both frequency and polar-

ization information at 19 and 37 GHz. The spatial and temporal variations of the ice temperature are taken into account by the NTA to the first order by using the polarization ratio (PR) and the spectral gradient ratio (GR) which are defined by

$$PR = \frac{TB(19V) - TB(19H)}{TB(19V) + TB(19H)} \quad (1)$$

$$GR = \frac{TB(37V) - TB(19V)}{TB(37V) + TB(19V)} \quad (2)$$

where, for instance, $TB(19V)$ is the vertically polarized brightness temperature at 19 GHz, and H refers to horizontal polarization. The two nearly independent parameters PR and GR are used to solve a mixing equation for the three dominant ocean surface types of the Arctic: open water, first-year and multiyear ice. The NTA is commonly used in combination with a filter, based on a combination of the 19 and 22 GHz SSM/I channels (Cavalieri *et al.*, 1995). This filter effectively reduces the spurious ice concentrations.

Comparisons of the NTA to a few other sea ice concentration algorithms basing on 19 and 37 GHz data conducted by Burns (1993) and Comiso *et al.* (1997), reveal discrepancies of up to 45% in the ice concentration values. The NTA has a few shortcomings, for instance the underestimation of the ice concentration in presence of new ice and the low resolution of the 19 GHz channels. Recently, the NTA was enhanced by Markus and Cavalieri (2000) in order to overcome the problem of a bias towards lower ice concentrations associated with snow surface effects. The revised algorithm (NT2) includes the 85 GHz channels, which are less sensitive to inhomogeneities inside the snow. The NT2 algorithm has not been used in this study due to the lack of 85 GHz aircraft measurements.

The 85 GHz SSM/I channels yield considerably higher resolution than the other SSM/I channels. However, the atmosphere is far more opaque at 85 GHz compared to 19 and 37 GHz, and can cause severe biases in geophysical surface parameters obtained from 85 GHz SSM/I data, particularly in cloud-covered areas. However, if the atmospheric conditions are obtained from other sources, or have negligible variations in the region studied, the 85 GHz channels can well be used for sea ice observations.

A procedure to retrieve the total sea ice concentration from a spaceborne dual-polarized passive microwave instrument operating near 90 GHz was first developed by Svendsen *et al.* (1987). A physical basis to interpret 85 GHz brightness temperature in terms of total and multiyear ice concentration was presented by Lomax *et al.* (1995). They compared the Svendsen *et al.* algorithm (SVA) and the NTA estimates of total ice concentrations and found an excellent agreement ($\pm$ 3 %) over cloud-free areas of high ice concentration in winter. The agreement remained good ($\pm$ 6 %) for cloudy scenes in winter but larger discrepancies occurred in summer. Lubin *et al.* (1997) compared ice concentrations retrieved from 85 GHz SSM/I data using the SVA with shipborne ice observations during Arctic summer and found an agreement that was at least as good as that obtained with NTA ice concentrations. Markus and Burns (1995) and Hunewinkel *et al.* (1998) developed methods to derive the sea ice edge and to detect polynyas with the spatial resolution of the 85 GHz SSM/I channels and the weather-influence sensitivity of the 37 GHz SSM/I channels. These methods can not be used to calculate the sea ice concentration, but to classify open water, the interior ice pack, and new ice.

Kern (2000) developed a weather-correcting algorithm (SEA LION algorithm) to calculate the total sea ice concentration using the polarization ratio at 85 GHz together with monthly tie points, which are reference brightness tem-

peratures for the two ocean surface types of the Antarctic: open water and ice. The SEA LION algorithm includes a weather correction scheme based on radiative transfer modelling and atmospheric data calculated from the other SSM/I channels or taken from numerical weather prediction models. Kern and Heygster (2001) compared the SEA LION, NTA, and Bootstrap algorithm (BTA) (Comiso *et al.* 1997) ice concentrations in the Antarctic. Taking advantage of the finer spatial resolution of the 85 GHz channels, SEA LION sea ice concentration maps show by far more detail. On these maps the sea ice edge in the MIZ and in polynyas can be located within 10 km accuracy as was shown in comparison with independent data. The SEA LION sea ice concentration of the Antarctic averaged over the period 1992-99 mediates between those obtained with the NTA and the BTA, being closer to the latter one. Therefore, according to the results of Comiso et al. (1997), using the SSM/I 85 GHz channels can provide a more realistic view of the Antarctic sea ice conditions. However, the quality of the SEA LION ice maps strongly depends on the reliability of the involved atmospheric data.

3.1 ASI algorithm

The ARTIST Sea Ice (ASI) algorithm is a hybrid algorithm combining the SVA used for ice-covered regions with the NTA algorithm used for the ice-free ocean. This approach takes advantage of the low sensitivity of the 19 GHz channels to atmospheric effects and of the high resolution of the 85 GHz channels.

The foundation of the basic equations and a detailed discussion of the atmospheric opacity at 85 GHz can be found in Svendsen et al. (1987) and in Lubin et al. (1997). Therefore, we limit our description of the SVA to a level useful for a practical implementation.

The microwave radiative transfer equation is expressed in a simplified form as defined in Svendsen *et al.* (1987)

$$\begin{aligned} P &= c(aC + b), \\ a &= \Delta e_{ice} T_{ice} - \Delta e_{water} T_{water}, \\ b &= \Delta e_{water} T_{water}, \\ c &= (1.10 e^{-\tau} - 0.11) e^{-\tau} \end{aligned} \tag{3}$$

where C is the total sea ice concentration, P is the difference between the vertically and horizontally polarized 85 GHz brightness temperatures, Δe is the difference in surface emissivity between vertical and horizontal polarization for the ice or water surface fraction, and tau is the total atmospheric optical depth. Equation (3) was derived assuming a plane parallel atmosphere over a Lambertian surface with the effective temperature being constant with height and with a viewing zenith angle near 50°.

Tie points are defined through the conditions for the totally ice-free $C(P_0) = 0$ and ice-covered ocean $C(P_1) = 1$. Inserting the tie points in equation (3) leads to an equation system which can be formulated using the partial derivatives of the total sea ice concentration $\frac{\partial C}{P}$.

$$\frac{\partial C(P)}{P}|_{C=0} = \frac{b}{aP_0} \tag{4}$$

$$\frac{\partial C(P)}{P}|_{C=100} = \frac{1 + b/a}{P_1} \tag{5}$$

for totally ice-free (eq. 4) and ice-covered (eq. 5) ocean.

The ratio b/a=-1.14 given by Svendsen for typical sea ice signatures has been assumed to be constant.

The basic assumption of the SVA is that the atmospheric influence can be represented by a smooth function of C between the ice and the ice-free ocean. Therefore, the third-order polynomial function

$$C(P) = d_3 P_3 + d_2 P_2 + d_1 P + d_0 \qquad (6)$$

is then used throughout the image to evaluate the total ice concentration at each pixel. This is an approximation to take into account areas of intermediate concentrations where equations (4) and (5 are not defined. The coefficients d_i can be derived from prescribing $C(P)$ with $C(P_0) = 0$ and $C(P_1) = 1$ as well as equations (4) and (5).

Svendsen *et al.* (1987) and Lubin *et al.* (1997) suggested to use the 85 GHz algorithm in conjunction with lower frequency observations to reduce large errors caused by weather effects. We follow these suggestions by introducing a low frequency weather-filter over ice-free areas in order to derive the sea ice concentration C(ASI).

Applying the following rule to each pixel of ice concentration maps derived with the SVA and the NTA:

$$\begin{aligned} C(ASI) &= 0 &&, C(NTA) \leq T \\ C(ASI) &= C(SVA) &&, C(NTA) > T \end{aligned} \qquad (7)$$

C(NTA) and C(SVA) are the ice concentrations calculated with the NTA and the SVA, respectively, and T=30% is a threshold to masks ice-free areas as obtained with the NTA. The NTA has been used in combination with the weather filter described in Cavalieri *et al.* (1995).

For this approach, C(SVA) and C(NTA) have to be mapped into the same grid. For the present study we use a polar stereographic projection according to Snyder (1982) and a gridding and interpolation method, which is part of the free software package Generic Mapping Tools GMT (Wessel and Smith, 1998; (`http://imina.soest.hawaii.edu/gmt/`). In order to generate a smooth and differentiable interpolation the gridding was performed with continuous curvature splines in tension (Smith and Wessel, 1990). We used a grid cell size of 200 m for comparisons between ice concentrations derived from aircraft and from SSM/I measurements as well as between SSM/I and ERS-2 SAR data. A grid cell size of about 8 km was used to ingest the SSM/I ice concentrations into the numerical atmospheric models.

The sea ice edge obtained from the 19 GHz channel data can be expected to be located farther away from the pack ice if compared to 85 GHz channel data. For instance C(SVA) may be already 0% while C(NTA) still is 30% (see Fig. 6). In general the full range (0-100%) of ice concentrations is detectable despite of the rigid threshold cut-off T=30% (eq. 7).

The local variability of the atmosphere and the radiation properties of water and ice are not considered using the SVA. A detailed analysis of the resulting errors was done by Svendsen *et al.* (1987) and by Lubin *et al.* (1997).

The proposed combination (eq. 7) removes most weather-induced ice concentrations in the open sea. But there remain problems near the ice edge. A passing front, for instance, causes an abrupt cut-off at the ice edge. Very sharp ice concentration gradients can signalize these weather-induced errors. It is possible to distinguish these effects from an actual compacted ice edge with the knowledge of the temporal development and the prevailing weather conditions. The additional usage of cloud signature maps, a new method developed by Miao *et al.* (2000), can significantly improve the detection of regions with false ice concentration values. The removal of errors due to the local atmospheric effects is not provided by the SVA. A detailed discussion of a local weather correction method can be found in Kern (2000). The usage of the ASI sea ice maps is therefore limited to a range of applications, for instance, case studies for which the atmospheric conditions are well known or within a data assimilation framework where one can deal with such errors as statistical noise.

The selection of proper tie points P_0 and P_1 is crucial, because they include the complete radiative physics empirically. In order to account for the variability of the atmosphere, Svendsen *et al.* (1987) proposed a self-adapting method to calculate tie points for each orbit separately by "setting P_1 equal to the median of a certain number of the smallest P, and P_0 equal to the median of the largest P".

Svendsen's method has been found to be vulnerable to cloud cover contamination for which the algorithm is intended to correct. Lubin *et al.* (1997) reported that there can be large fluctuations in the polarization for both open water and sea ice, such that the absolut highest (lowest) polarization may not represent the best tie point for 100% open water (100% ice). In order to overcome this problem they recommend the help of ancillary data such as a clear-sky visible/infrared satellite image.

We propose a new method for the estimation of 85 GHz tie points which avoids the a priori selection of regions well inside and well outside the sea ice. This method does not depend on clear-sky visible/infrared satellite images and involves reference ice concentration data $C(\mathrm{x})$ obtained using a well-proven method instead. These $C(\mathrm{x})$ data can be based on SSM/I data as well as on measurements of any other satellite or airborne sensor which has observed the same area with only a few hours difference to the SSM/I overpass. We assume that the validated reference algorithm provides sea ice concentrations which can be used as ground truth data. The reference values have to cover a sufficient range of different ice concentrations in order to minimize the least-squares regression error.

The data have to be on the same grid with matched resolution (degraded for the higher resolution data). Our proposed method includes the following steps:

1. Choose initial tie points P_0 and P_1.
2. Calculate the sea ice concentration $C(\mathrm{ASI})$.
3. Calculate the least-squares fit parameters SLOPE and OFFSET from $C(\mathrm{x})$ and $C(\mathrm{ASI})$.
4. Vary the tie points P_0 and P_1.
5. If not (SLOPE$\approx$1 and OFFSET$\approx$0) goto 2.

Hereby $C(\mathrm{ASI})$ is the ice concentration defined by eqs. (6) and (7). The estimation of tie points by calculating the minimum and maximum values of some samples implies the samples to be suitable and well distributed, which in general may be not the case. The usage of a least-squares statistics with independent reference data rather than the selection of just two points should provide more robust and accurate results for the tie points, as the results shown in the next section will confirm.

4 Validation

The ice concentrations derived from aircraft measurements have been taken as a reference in order to obtain the tie points P_0 and P_1 of the ASI algorithm with the previously described least-squares method. When comparing aircraft and satellite data the different spatial resolutions of the sensors have to be taken into account. In order to adjust the aircraft data to the effective field of view of the SSM/I, they have been smoothed with a Gaussian weighted filter. In the following the results of April 1st (microwave radiometer) and 4th (optical line scanners) are discussed in more detail.

We conclude this section with a statistical comparison of the ASI and NTA ice concentrations, both derived from SSM/I, for the whole ARTIST period (March 9 till April 10).

4.1 Validation with aircraft passive microwave measurements

A cloud free situation south-east of Svalbard on April 1st was used to fly three long legs over the ice edge zone in Storfjorden. The flight track of the Polar 4 aircraft is shown in Figure 1.

The measurements started at 10:45 and ended at 14:45 UTC yielding profiles of surface microwave radiances. The measurements were interrupted by calibrations. Therefore, the total duration of the sea ice concentration time-series shown in Fig. 2 and 4 is reduced to about three hours corresponding to a total distance of 689 km.

Ice concentrations were derived from the AWI radiometer data with the NTA algorithm, henceforth denoted aircraft data C(ar;NTA).

In order to check their consistency C(ar;NTA) values have been compared to ice concentrations derived with the NTA from SSM/I data C(SSM/I; NTA).

The mean difference between C(ar; NTA) and C(SSM/I; NTA) is less than one percent (-0.5%) with a standard deviation of 5% (Fig. 2). The least-squares fit of both resolution-matched data sets yields (Fig. 3):

$$C(ar;NTA) = 1.0818C(SSM/I;NTA) - 0.06$$

The same set of tie points (see Cavalieri *et al.*, 1991) has been used for aircraft and satellite data. The atmospheric influence for the flight level of the SSM/I is included into the NTA tie points. This might cause problems since SSM/I data include the atmospheric influence of the entire atmospheric depth while aircraft data are influenced by the atmospheric layer below the aircraft. The latter influence can be expected to be substantially smaller. However, the mean difference in the obtained ice concentrations is very small, especially for high concentrations, and therefore, the above-mentioned difference has been neglected in further calculations. Nevertheless errors are likely to occur in cases of a heavy cloud-cover since the aircraft measurements have been undertaken during clear-sky conditions.

In the next step, the aircraft data C(ar; NTA) have been used together with the SSM/I 85 GHz data in order to derive tie points for the ASI algorithm as previously described. The tie points which provide the best linear fit of about 55 data points (averaged aircraft ice concentration profiles and co-located SSM/I ice concentration pixels) are:

$$\begin{aligned} P_0 &= 47\text{K (open water)} \\ P_1 &= 7.5\text{K (sea ice)} \end{aligned}$$

From these tie points we obtain the coefficients for the third-order polynomial

$$\begin{aligned} d_0 &= 6.45714 * 10^{-6}, \\ d_1 &= -0.000605256, \\ d_2 &= -0.00922521, \\ d_3 &= 1.10031 \end{aligned}$$

and calculated ice concentrations (eqs. 6 and 7) henceforth denoted as C(SSM/I; ASI), C(ASI) or ASI data.

The mean difference between C(ar; NTA) and C(SSM/I; ASI) is less than one percent (-0.6%) with a standard deviation of 6% (Fig. 4). The correlation coefficient CC=0.97 between both data sets confirms the linear relationship of the results from the different sea ice algorithms NTA and ASI (Fig. 5). The above-mentioned tie points have been used for all days of this study except for April 4th and 5th where line scanner data was used.

4.2 Validation with optical line scanner measurements

On April 4th two research aircraft (Polar 2 and 4) flew a coordinated mission along the fifth

meridian in a convective atmospheric boundary layer (ABL) during a cold air outbreak. Sea ice information across the MIZ was obtained over a distance of 38 km on Polar 2 using the optical line scanner system.

The ice concentration derived from line scanner data C(al) were used in order to estimate the tie points for the ASI algorithm similarly as demonstrated in the previous section (Bochert, 1999):

$$P_0 = 50.2\text{K (open water)}$$

and

$$P_1 = 12.3\text{K (sea ice)}$$

From these tie points we derived the corresponding coefficients

$$\begin{aligned} d_0 &= 1.82546 * 10^{-5}, \\ d_1 &= -0.00196167, \\ d_2 &= 0.0362013, \\ d_3 &= 0.817535 \end{aligned}$$

and calculated ice concentrations C(SSM/I; ASI) (eqs. 4 and 7). These values were used for the atmospheric modelling studies on April 4th and 5th 1998. The mean difference between C(al) and C(SSM/I; ASI) is less than one percent (-0.4%) with a standard deviation of four percent.

4.3 Validation with satellite passive microwave measurements

We analysed the relationship between C(ASI) and C(NTA), both calculated from SSM/I data for an area of 325 x 325 km^2 centered at 80°N, 0° in the Fram Strait MIZ. About 30 SSM/I swaths during March 9th and April 10th were evaluated (not shown here). The resolution of C(ASI) data was reduced to those of the low frequency channels. Linear regression parameters and correlation coefficients were calculated for the two sets of tie points. The results summarised in Table 2 show that the averaged linear regression line for the NTA reference tie points is almost the identity. In consequence, it makes no difference whether ASI tie points were derived from aircraft or satellite NTA reference data. Vice versa, this opens the path to an automatic implementation of the proposed method without access to aircraft data.

The maximum deviation between the reduced-resolution ASI (with NTA reference tie points) and NTA ice concentration data was below 10% which legitimizes the usage of fixed tie points at least for the ARTIST region and period. The use of fixed tie points is also supported by Lubin *et al.* (1997) have also used fixed tie points and have show that consistent ice concentration estimates can be obtained without varying the tie points from one day to the next during arctic summer.

The ASI ice concentrations calculated with the tie points referenced to the optical sensor are on average 10% higher than those obtained with the NTA for regions well inside the ice. This agrees with comparisons of NTA sea ice concentration maps and optical satellite images reported by Steffen and Schweiger (1991) and Comiso *et al.* (1997).

In order to examine a possible influence by a change in the surface air temperature on the proposed method we have considered surface air temperature measurements of the ARTIST driftbuoy 9372 deployed by Polar 4 on March 5th. These measurements varied between -37° C and -2°C during March and April. We analysed the dependency of the above-mentioned analysis on the temperature and found none (CC=0.03) for the slope and a slight negative correlation (CC=-0.4) for the offset parameter.

However, the ARTIST data set covers a relatively short period and is limited to the environment of Svalbard which prevents the

generalization of the results. Therefore, we constructed automatic processing routines for the production of sea ice maps as a first attempt of using the proposed method throughout all seasons in both hemispheres (see `http://www.seaice.de` for daily ASI maps). But the evaluation of this data has not been done yet. Kern and Heygster (2001) analysed the seasonal variablility of the 85 GHz SEA LION algorithm sea ice tie points recommending the usage of monthly or at least seasonally varying sea ice tie points. Thus, a seasonal variability can also be expected for the ASI sea ice tie points and have to be considered for an extension of the method.

5 Comparisons to ERS-2 SAR images

There are no established algorithms available to estimate the ice concentration from ERS-SAR images due to the limitation of: only one vertically polarized C-band channel, the steep incidence angle, ambiguities in sea ice surface and volume scattering effects, wind speed depending ocean clutter and the presence of speckle noise (Bochert, 1999). Nevertheless, ERS-SAR images carry valuable spatially high-resolution information, which can be accessed by visual inspection. In this study, ERS-2 SAR images have been used in a more qualitative manner for a consistency check. We present two local case studies observed with ERS-2 SAR and SSM/I: the MIZ in the Fram Strait and the Storfjorden Polynya.

5.1 Evolution of the MIZ in the Fram Strait

The advantage of the finer resolution of SSM/I observations when using the 85 GHz channels is demonstrated with two different ERS-2 SAR images obtained in the Fram Strait north-west of Svalbard.

A compact ice edge zone resulting from on-ice flow during the previous days is evident in the ERS-2 SAR image of March 30th, 1998 (Fig. 6, top). Then a low pressure system east of Svalbard and high pressure over Greenland has lead to northerly winds shifting the ice edge southwards and transforming the formerly compact ice edge zone into a diffuse one (Fig. 6, bottom).

The average distance between the 30% and 60% isolines was taken as a measure for the width of the MIZ and is shown in Table 3. The sharp gradient of the ASI ice concentration on March 30th decreases during the week and has changed by a factor of 3.5 on April 6th. In comparison, the NTA ice concentration gradient has changed less (factor 1.6) because of the lower spatial resolution of the 19 GHz channels.

The difference in the spatial resolution is exemplified by the number of independent measurements for the 5000 km^2 area which is shown in the top image of Figure 6; this area is covered about twice (32 fold) by the effective field of view of the 19 GHz (85 GHz) channels.

5.2 Storfjorden Polynya

A persistent latent heat polynya in Storfjorden, Svalbard, was observed by ERS-2 SAR imagery during the winter 1997/1998 (Haarpaintner, 1999). Since the temporal coverage of Storfjorden by ERS-2 SAR data is of the order of two weeks, the ERS-2 SAR observations were combined with polynya models and in situ data to quantitatively describe the importance of the polynya for the total ice production and bottom water formation from induced brine release in this area (Haarpaintner *et al.*, in press).

In order to replace or support the rather infrequent SAR observations with an approach, which allows more frequent observations, we made some initial attempts of using SSM/I data for this purpose. Figure 7 presents the ice

conditions in Storfjorden on April 9th, 1998, observed with ERS-2 SAR. We manually segmented the ERS-2 SAR image of Figure 7 in order to derive a thematic map consisting of three classes: fast ice, pack ice and polynya (Haarpaintner, 1999). The polynya class was defined in a fuzzy sense, and contains brash ice, new ice, nilas or young ice in addition to open water areas. A more concise classification of the polynya ice types is not feasible using ERS-2 SAR images due to ambiguities of the radar backscatter. The thematic map is shown in Figure 8 together with ice concentration isolines derived from SSM/I data with the NTA and the ASI algorithm. The northern part of the fjord (north of 78 °N) and the eastern coast of Spitsbergen were covered by fast ice of about 120 cm thickness. A flaw polynya developed from the fast ice southwards to about 77° 30' N. Similar conditions were observed from a helicopter flight during fieldwork on April 15th, 1998. According to the observations and the polynya models, the Storfjorden polynya was composed by about equal areas of open water and thin ice, which is in good agreement with the average ASI ice concentrations.

6 Modelling of the atmospheric boundary layer over the marginal sea ice zone near Svalbard

The heat exchange between atmosphere and ocean is strongly influenced by the sea ice concentration. Regional atmospheric models use grid sizes of about 20 km and thus ice concentration data are needed in a similar resolution. In the following two subsections the results of two different mesoscale atmospheric models are discussed. The principal improvements that can be expected from high resolution ice data, such as obtained from the ASI algorithm, are further demonstrated.

6.1 Flow parallel to the ice edge over Storfjorden

The air flow over the ice-edge zone in Storfjorden was simulated using a two-dimensional hydrostatic mesoscale ABL model (Savijärvi, 1991). The present model version has 92 points with a 2 km grid length in the horizontal, and 50 levels in the vertical, and the flow is forced by a geostrophic wind at a height of 3 km (in this case based on the aircraft observations and analyses of the operational model HIRLAM). The sea ice concentration is prescribed and applied when calculating the grid-averaged surface fluxes by the mosaic method (Vihma, 1995).

On March 30th, 1998, an aircraft flight mission was made over the Storfjorden (Hartmann *et al.*, 1999): it was observed that the ABL flow was parallel to the ice edge, and the leads were 10 to 20 K warmer than the near-surface air. Two otherwise identical model simulations were made: in the first one the ice concentration was based on the ASI algorithm, and in the second one on the NTA. The ice concentrations differed substantially from each other, the NTA producing a more diffuse ice edge zone (Fig. 9 a). The results of the observed and modelled air temperature at a height of 40 m are shown in Figure 9 b. We see that the air temperature is closely related to the ice concentration in both simulations. The observed air temperature has a strong gradient in the ice edge zone. This is well reproduced in the simulation based on the ASI data but not in the one based on the NTA. In the zone where the ice concentrations differ from each other (from -60 to 70 km in Fig. 9), the mean absolute deviation between the observed and modelled air temperature is 0.7 K for the ASI-based results and 1.7 K for the NTA-based results. In the 50 km wide zone of the largest difference, the

corresponding numbers are 0.8 K and 3.1 K, respectively.

6.2 Off-ice flow over the Fram Strait

The non-hydrostatic mesoscale model METRAS (Schlünzen, 1990; Lüpkes and Schlünzen, 1996) was applied in a 2D version to simulate the flow across the MIZ northwest of Svalbard at about 80° N 7° E using a horizontal resolution of 8 km and 14 grid layers below 500 m height. Figure 10 shows a comparison of aircraft observed ice concentration C(al) data with satellite estimates C(SSM/I; NTA) and C(SSM/I; ASI). Obviously the NTA algorithm underestimates the concentration for values higher than 0.5 whereas ASI data (interpolated on the model grid) are close to the observations.

On April 5th, 1998, a cold-air outbreak had developed with off-ice northerly winds across the MIZ. These conditions always lead to strong convection over the MIZ due to the large difference between the near-surface air temperature and that of the water surface. Figure 11 shows the profiles of the potential temperature as observed by the aircraft at the positions marked by the crosses in Fig. 10, and model results which have been obtained with the NTA or ASI algorithm sea ice concentrations.

The first profile refers to the northernmost position at -40 km in Figure 10, the profile on the right hand side is at the southern end of the MIZ (position 22 km). It is quite obvious that observations and model results are in better agreement when using the ASI ice concentrations C(SSM/I; ASI). A similar result was obtained for the April 4th, 1998 (not shown here).

Discussion and conclusions

Aircraft flights in March and April 1998 during the Arctic Radiation and Turbulence Interaction Study provide high resolution sea ice data. We used the NASA Team algorithm (NTA) to derive ice concentrations from aircraft-based dual-polarized 19 and 37 GHz radiometer data and to verify and validate a hybrid SSM/I algorithm. The ARTIST Sea Ice (ASI) algorithm combines the high resolution (12 km) of the 85 GHz channels with the lower sensitivity of the NTA to the weather influence for reliable open water/ice discrimination.

Tie point selection for Svendsen's ice retrieval method has been critical because of the large atmospheric opacity at 85 GHz. We present a new method which requires reference ice concentration data from a validated algorithm, such as the NTA.

We derived tie points for the ASI algorithm with the aid of a linear regression method and aircraft data. By that way unreliable a priori guesses of regions well inside and well outside the ice have been avoided.

Very high correlations CC=0.97 and CC=0.98 have been obtained from a 689 km aircraft profile and co-located SSM/I ice concentration pixels calculated with the NTA and the ASI algorithm, respectively. The mean differences between aircraft and satellite data were less than one percent for both algorithms with standard deviations of about five percent.

We derived an alternative set of tie points for the ASI algorithm by using aircraft optical line scanner images. Ice concentrations calculated with the ASI algorithm and these tie points were not afflicted with low concentration biases typically associated with the presence of thin ice types as those obtained with the NTA.

We compared NTA and reduced-resolution ASI ice concentrations, both calculated from SSM/I data. The ASI tie points have been chosen with reference to aircraft NTA and optical line scanner ice concentration data, respectively. The results indicate a strong linear relationship of ASI and NTA data. The NTA

underestimates high ice concentrations by 10% on average with respect to the ASI data, calculated with optical line scanner reference tie points. The linear regression line for the ASI algorithm, calculated with aircraft NTA reference tie points, and the SSM/I NTA ice concentration data is close to the identity for every day during March and April, 1998. This point is interesting from a practical point of view for situations without access to aircraft data for the estimation of tie points for the ASI algorithm; it makes hardly any difference whether the reference data stem from aircraft or satellite. Therefore, it should be possible to determine ASI tie points from SSM/I data automatically.

The proposed method for ASI tie point estimation should work in almost the same manner with any other sea ice algorithm, for instance with the revised NASA Team algorithm NT2. Svendsen's near 90 GHz model depends on two parameters (tie points) only. Thence it is non-ambiguous to adjust these parameters in order to match the perfect linear fit with any reference ice concentration data.

We used ERS-2 SAR images to support qualitatively the interpretation of ASI and NTA sea ice maps. We found that the 85 GHz channels are suitable to resolve mesoscale ice features. We demonstrated how the state of the ice edge (diffuse or compact) can be observed in ASI ice maps. Moreover, we found that the 85 GHz channels are suitable for the observation of coastal zone polynyas.

We investigated the heat budget of the atmospheric boundary layer (ABL) with numerical simulation models in different two case studies: on March 30th 1998, in the Storfjorden, the wind was parallel to the ice edge, while on April 5th an off-ice flow took place over the Fram Strait. In both studies the model runs applying the ice concentration data based on the ASI algorithm agreed better with the observations than those based on the NTA data. It is interesting to note that the ABL was sensitive to the ice concentration data of two very different cases. Furthermore, the results were obtained using two different models: a hydrostatic one with a first-order turbulence closure and a non-hydrostatic one with an advanced turbulence closure. Thus, the importance of the spatial resolution of the sea ice concentration data in ABL models is neither restricted to certain flow conditions nor to a certain kind of atmospheric models. From the point of view of both operational and research applications, we believe that high-resolution modelling of the atmosphere over the polar oceans is relevant only when the model boundary conditions are based on accurate data on the ice concentration, or at least on the accurate location of the ice edge.

We conclude that the ASI algorithm is practical for field studies where extensive high resolution ice concentration data are required and some independent ice concentration measurements are available for the estimation of well adapted tie points. The calculation of the ice concentrations is quite simple and straightforward, thus the operational usage of the ASI algorithm is feasible (see http://www.seaice.de). However, the validity of ASI results depends on the weather conditions. For instance, passing fronts may cause large errors in the obtained ice concentrations. And there is an obvious need for further validation studies, especially for other regions, seasons, and weather conditions.

Acknowledgments

The authors are grateful to all the people who contributed to the successful completion of the ARTIST campaign. In particular, we thank the crew of the Polar 2 and 4 research aircraft. We also thank Pete Conway of Earth Systems Science Lab at the University of Alabama, Huntsville, for providing SSM/I ground pass times which were used for flight planning; Sören Andersen of the Danish Meteorological Institute for the recording of the SSM/I single swath data; Stefan Kern of the Institute of Environmental Physics, University of Bremen, Germany, for numerous comments and discussions; Klaus Künzi for hosting Lars Kaleschke in the Institute of Environmental Physics, University of Bremen, Germany.

The ARTIST project was funded by the Commission of the European Community under contract Nr. ENV4-CT97-0497-0487 (DG12-ESCY).

The Storfjorden work was funded by grant contract Nr. MAS3-CT96-5036 from the Commission of the European Community and grant of Norwegian research council 127802/720 under contract with the Norwegian Polar Institute, Tromsö.

ERS2-SAR images of Storfjorden were distributed by the Tromsö Satellite Station and weather data from Hopen by the Norwegian Meteorological Institute (DNMI).

References

Aagaard, K., and Carmack, E.C. (1989). The role of sea ice and other fresh water in the arctic circulation, *Journal of Geophysical Research*, Vol 94, No. C10, pp. 14485-14498.

Bochert, A. (1999). Airborne line scanner measurements for ERS-1 SAR interpretation of sea ice, *International Journal of Remote Sensing*, Vol. 20, No. 2, pp. 329-348.

Birnbaum, G. , and Lüpkes, C. (submitted). A new parameterization of surface drag in the marginal sea ice zone, *submitted to Tellus*, 2000.

Burns, B.A. (1993). Comparison of SSM/I ice-concentration algorithms for the Weddell Sea, *Annals of Glaciology*, Vol. 17, pp. 344-350.

Cavalieri, D.J., Gloersen, P., and Campbell W.J. (1984). Determination of sea ice parameters with the NIMBUS 7 SMMR, *Journal of Geophysical Research*, Vol. 89, No. D4, pp. 5355-5369.

Cavalieri, D.J., Crawford, J.P., Drinkwater, M.R., Eppler, D.T., Farmer, L.D., Jentz, R.R., and Wackerman, C.C. (1991). Aircraft Active and Passive Microwave Validation of Sea Ice Concentration From the Defense Meteorological Satellite Program Special Sensor Microwave Imager, *Journal of Geophysical Research*, Vol. 96, No. C12, pp. 21989-22008.

Cavalieri, D. J., and Martin. S. (1994). The contribution of Alaskan, Siberian and Canadian coastal polynyas to the halocline layer of the Arctic Ocean, *Journal of Geophysical Research*, Vol. 99, No. C9, pp. 18343-18362.

Cavalieri, D. J., St. Germain, K. M., and Swift, C. T. (1995). Reduction of weather effects in the calculation of sea-ice concentration with the DMSP SSM/I, *Journal of Glaciology*, Vol. 41, No. 139, pp. 455-464.

Comiso, J.C., Cavalieri, D.J., Parkinson, C.L., and Gloersen, P. (1997). Passive Microwave Algorithms for Sea Ice Concentration: A Comparison of Two Techniques, *Remote Sensing of the Environment*, Vol. 60, pp.

357-384.

Haarpaintner, J. (1999). The Storfjorden polynya: ERS-2 SAR observations and overview, *Polar Research*, Vol. 18, No. 2, pp. 175-182.

Haarpaintner, J., Gascard, J.-C., and P. M. Haugan. Ice production and brine formation in Storfjorden, *Journal of Geophysical Research*, in press.

Hartmann, J., Albers, F., Argentini, S., Bochert, A., Bonafe, U., Cohrs, W., Conidi, A., Freese, D., Georgiadis, T., Ippoliti, A., Kaleschke, L., Lüpkes, C., Maixner, U., Mastrantonio, G., Ravegnani, F., Reuter, A., Trivellone, G., and Viola, A. (1999). Arctic Radiation and Turbulence Interaction Study (ARTIST), *Reports on Polar Research*, No. 305, Alfred-Wegener-Institute for Polar and Marine Res., Bremerhaven, Germany.

Hunewinkel, T., Markus, T., and Heygster, G.C. (1998). Improved Determination of the Sea Ice Edge with SSM/I Data for Small-Scale Analysis. *IEEE Transactions on Geoscience and Remote Sensing*, Vol. 36, No. 5., pp. 1795-1808.

Hollinger, J.P., Peirce, J.L., and Poe, G.A. (1990). SSM/I instrument evaluation. *IEEE Transactions on Geoscience and Remote Sensing*, Vol. 5, No. 28, pp. 781-790.

Kern, S. (2000). Sea ice concentration derived using SSM/I 85.5 GHz imagery. *Mapping and Archiving of Sea Ice Data - The Expanding Role of Radar*, JCOMM Technical Report No. 7, WMO/TD-No. 1027, pp. 179-184.

Kern, S., and Heygster, G. (2001). Sea ice concentration retrieval in the Antarctic based on the SSM/I 85.5 GHz polarization. *Annals of Glaciology*, in press.

Proc. of a Workshop on Mapping and Archiving of Sea Ice Data - The Expanding Role of Radar, JCOMM Technical Report No. 7, WMO/TD-No. 1027, pp. 179-184.

Kramer, H.J. (1996). *Earth Observation Remote Sensing*, 3rd edition, Berlin, Heidelberg, Germany: Springer-Verlag.

Ledley, T.S. (1988). A coupled energy balance climate - sea ice model: impact of sea ice and leads on climate, *Journal of Geophysical Research*, Vol. 93, No. D12, pp. 15919-15932.

Lubin, D., Garrity, C., Ramseier, R., and Whritner, R.H. (1997). Total Sea Ice Concentration Retrieval from the SSM/I 85.5 GHz Channels during Arctic Summer, *Remote Sens. Eviron.*, Vol. 62, pp. 62-76.

Lüpkes, C., and Schlünzen, K.H. (1996). Modelling the Arctic convective boundary layer with different turbulence parameterizations. *Boundary-Layer Meteorol.*, Vol. 79, pp. 107-130.

Schlünzen, K.H. (1990). Numerical studies on the inland penetration of see breeze fronts at a coastline with tidally flooded mudflats. *Beiträge zur Physik der Atmosphäre*, Vol. 63, pp. 244-256.

Markus, T., and Burns, B.A. (1995). A method to estimate subpixel scale coastal polynyas with satellite microwave data. *Journal of Geophysical Research*, Vol. 100, No. C3, pp. 16707-16718.

Markus, T., and Cavalieri, D.J. (2000). An Enhancement of the NASA Team Sea Ice Algorithm, *IEEE Transactions on Geoscience*

and Remote Sensing, Vol. 38., No. 3., pp. 1387-1398.

Martin, S., and Kauffman, P. (1981). A field and laboratory study of wave damping by grease ice, *Journal of Glaciology*, Vol. 27, No. 96, pp. 283-313.

Miao, J., Johnsen, K.P., Kern, S., Heygster, G., and Kunzi, K. (2000). Signature of Clouds over Antarctic Sea Ice Detected by the Special Sensor Microwave/Imager, *IEEE Transactions on Geoscience and Remote Sensing*, Vol. 38, No. 5, pp. 2333-2343.

Savijärvi, H. (1991). The United States Great Plains diurnal ABL variation and the nocturnal low-level jet, *Monthly Weather Review*, Vol. 119, No. 3, pp. 833-840.

Snyder, J.P. (1982). Map Projections Used by the U.S. Geographical Survey, *Geological Survey bulletin 1532*, Second edition, United States Government Printing Office, Washington.

Wessel, P., and Smith, W.H.F. (1998). New, improved version of Generic Mapping Tools released, *EOS Transactions American Geophysical Union*, Vol. 79, No. 47, pp. 579.

Smith, W. H. F, and Wessel, P. (1990). Gridding with continuous curvature splines in tension, *Geophysics*, No. 55, pp. 293-305.

Steffen, K., and Schweiger, A. (1991). NASA team algorithm for sea ice concentration retrieval from defense meteorological satellite program Special Sensor Microwave Imager: Comparison with Landsat imagery, *Journal of Geophysical Research*, Vol. 96, No. C12, pp. 21971-21987.

Svendsen, E., Mätzler C., and Grenfell, T.C. (1987). A model for retrieving total sea ice concentration from a spaceborne dual-polarized passive microwave instrument operating near 90 GHz, *International Journal of Remote Sensing*, Vol. 8, No. 10, pp. 1479-1487.

Vihma, T. (1995). Subgrid parameterization of surface heat and momentum fluxes over polar oceans, *Journal of Geophysical Research*, Vol. 100, No. C11, pp. 22625-22646.

Frequency [GHz]	Resolution [km^2]
19.35	69 x 43
22.235	60 x 40
37.0	37 x 29
85.5	15 x 13

Table 1: Effective field of view of the SSM/I channels. (Hollinger, 1990)

ASI tie point reference	Slope	Offset	Correlation
Aircraft passive microwave (NTA)	1.01 $\pm$ 0.04	-0.005 $\pm$ 0.015	0.99 $\pm$ 0.005
Optical line scanner	0.92 $\pm$ 0.02	-0.02 $\pm$ 0.01	0.99 $\pm$ 0.004

Table 2: Relationship between SSM/I ASI and NTA ice concentration data.

Algorithm	Resolution	Date	State	Width	Change
ASI	12 km	March 30th	Compact	6.6 km	-
ASI	12 km	April 6th	Diffuse	23.3 km	3.5x
NTA	50 km	March 30th	Compact	24.5 km	-
NTA	50 km	April 6th	Diffuse	38 km	1.6x

Table 3: Changes in MIZ width as observed from space with different spatial resolutions.

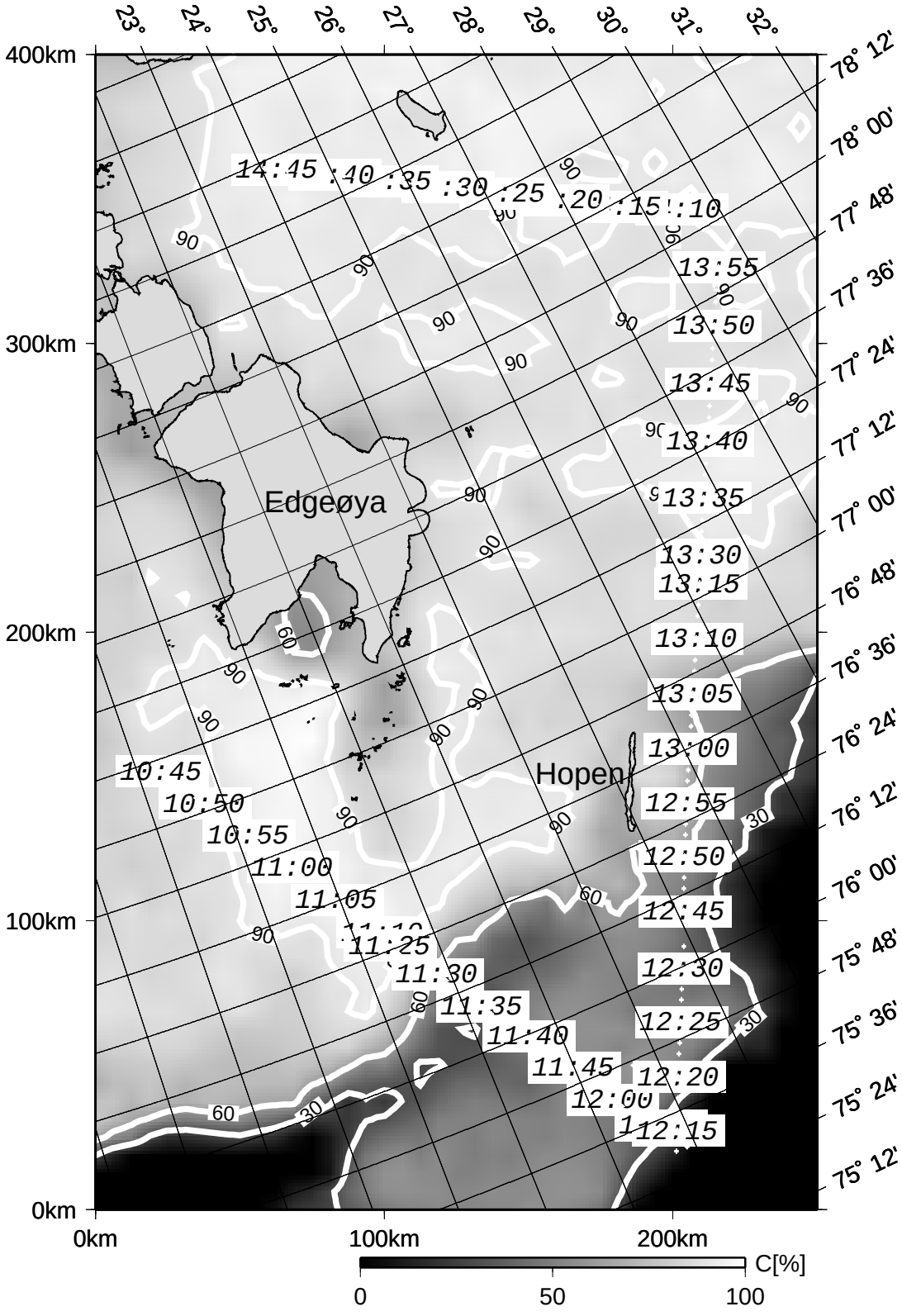

Figure 1: Flight track of the AWI Polar 4 research aircraft operating the dual-polarized 19 and 37 GHz AWI radiometers superimposed on the sea ice concentration map calculated with the ASI algorithm. Isolines of the sea ice concentrations are given in addition. The area shown is mainly covered with first-year ice. Only the area south of Hopen island consists of pancake ice.

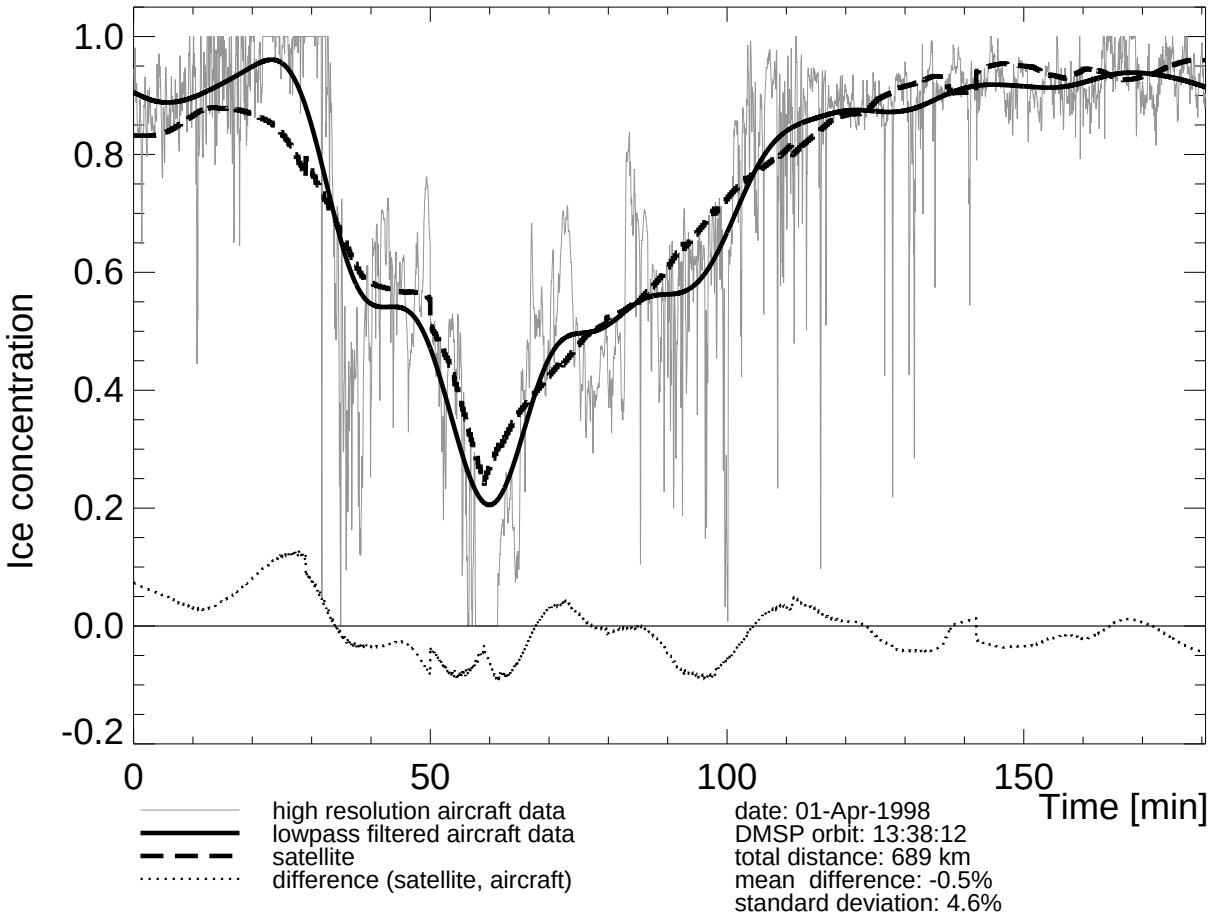

Figure 2: Ice concentrations C(ar; NTA) and C(SSM/I; NTA) derived from aircraft and satellite measurements using the NTA. The difference between the SSM/I and the lowpass-filtered aircraft data is also indicated. The time-series were constructed from seven measurement intervals of the profile shown in Figure 1 (10:43-11:12, 11:24-11:45, 11:59-12:08, 12:12-12:33, 12:44-13:16, 13:26-13:57, 14:09-14:47). For this reason slight disconuities appear in the curve obtained from the satellite profile.

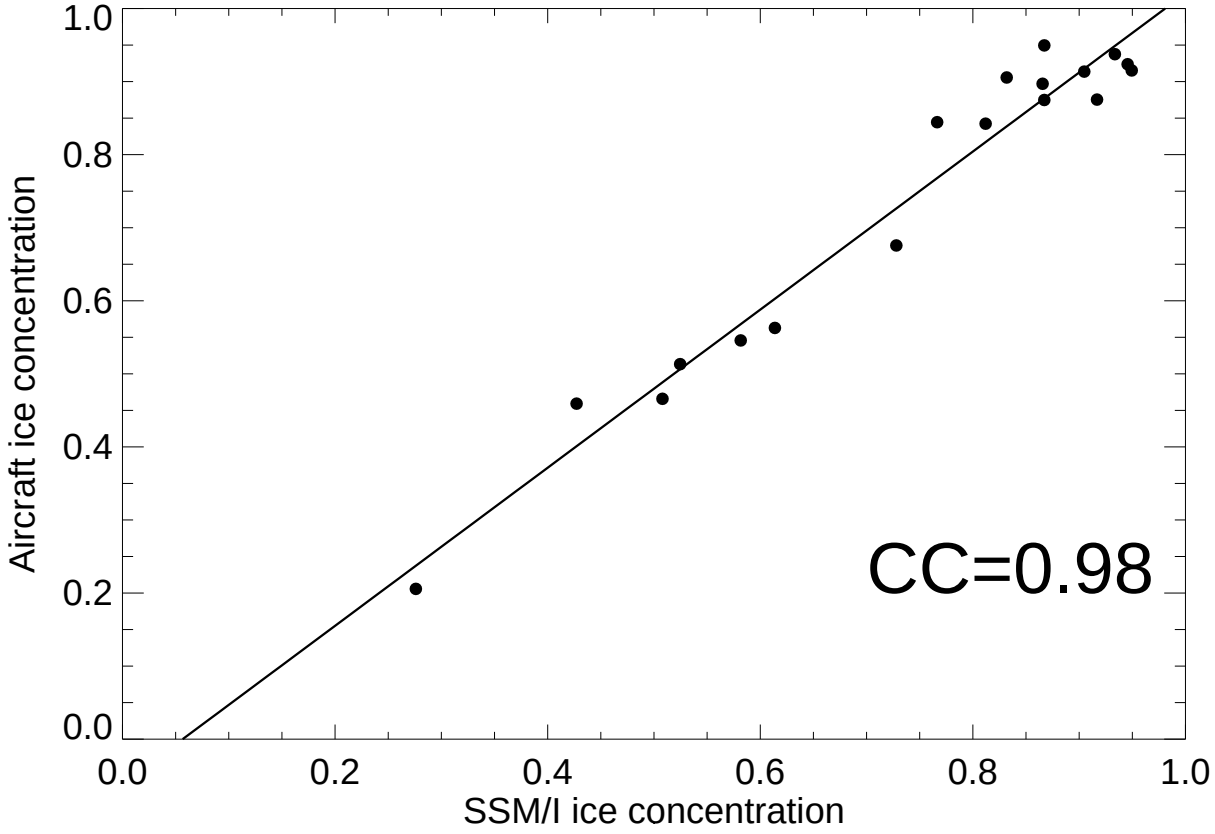

Figure 3: Average sea ice concentration obtained from aircraft data C(ar; NTA) and the co-located SSM/I ice concentration C(SSM/I; NTA).

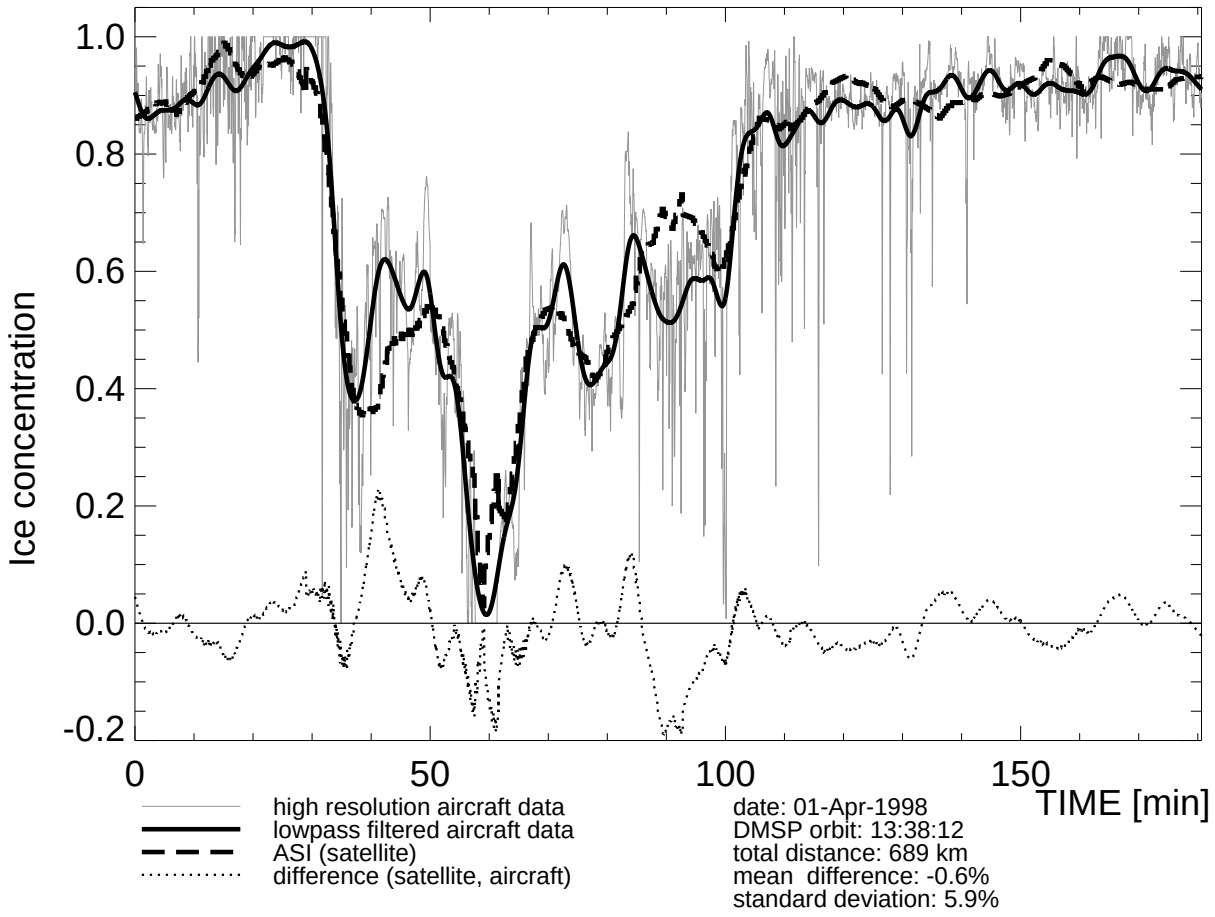

Figure 4: Ice concentrations C(ar; NTA) and C(SSM/I; ASI). The high resolution aircraft data are identical to those of Figure 2b.

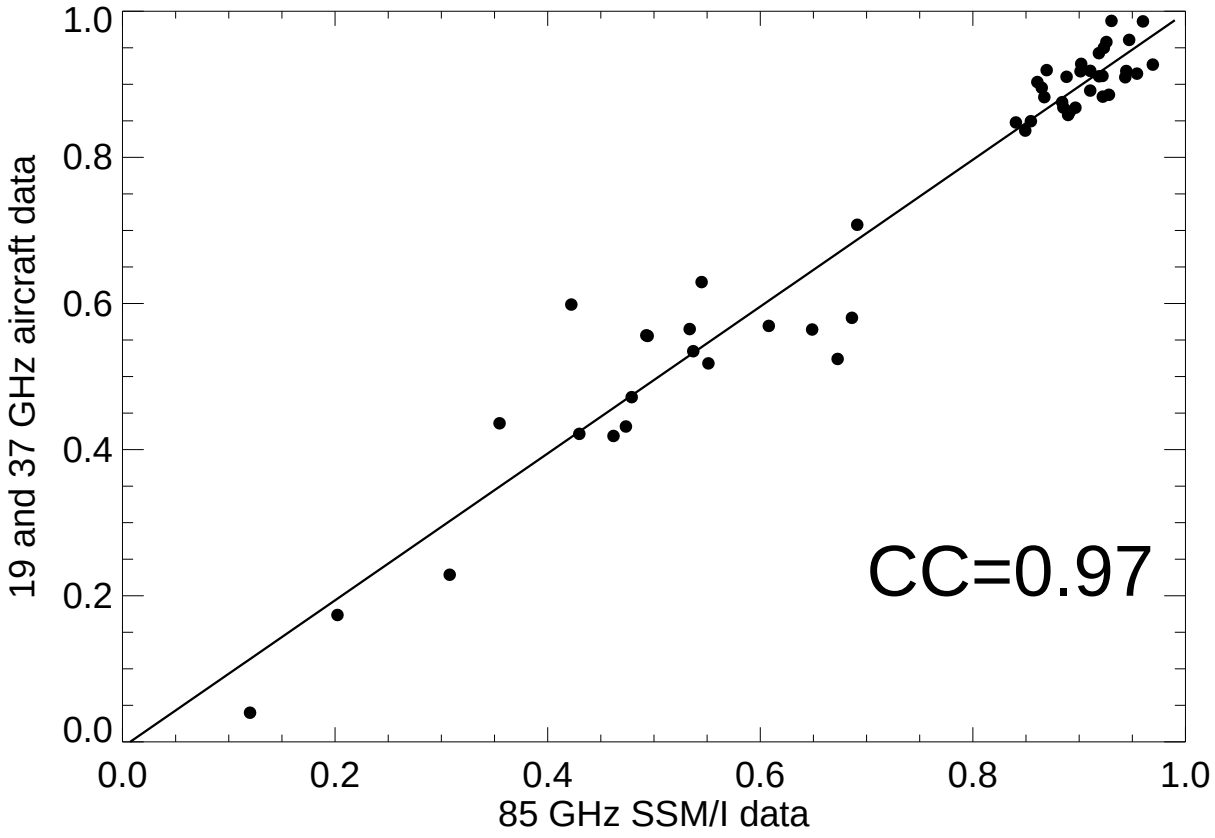

Figure 5: Average sea ice concentration obtained from aircraft data C(ar; NTA) and the co-located SSM/I ice concentration C(SSM/I; ASI). The high correlation coefficient proves the suitability of the ASI tie points for this case.

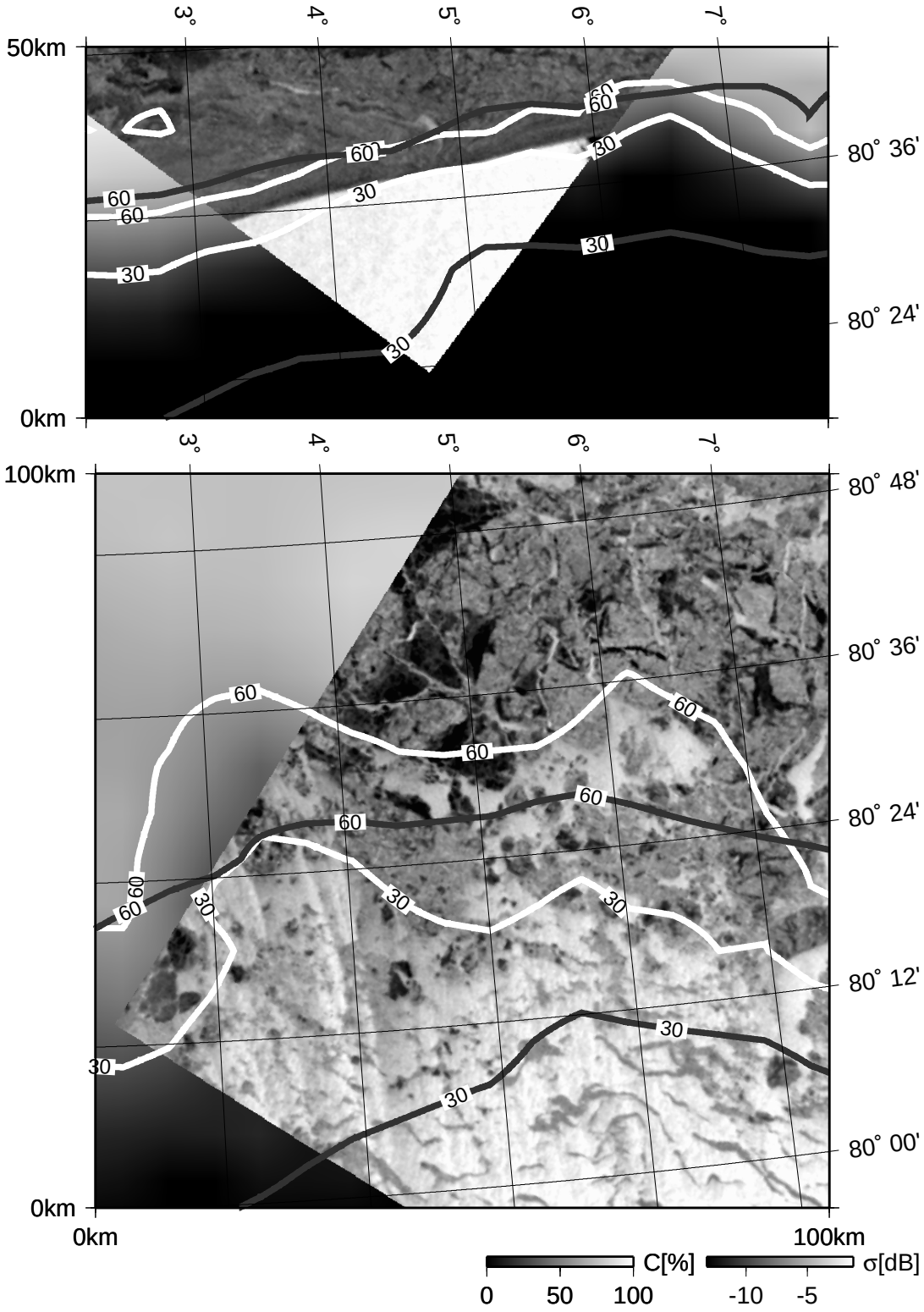

Figure 6: The marginal ice zone: SAR images recorded by the ERS-2 on March 30th, 1998 (top, orbit:15380, frame:1935) and on April 6th, 1998 (bottom, orbit:15480, frame:1953) The ERS-2 SAR images are overlaid by ice concentration isolines from the ASI algorithm (light) and NTA (dark). In areas not covered by the SAR images, the ice concentration C(SSM/I; ASI) is displayed in a gray scale. (Original ERS-SAR images (C)ESA 1998).

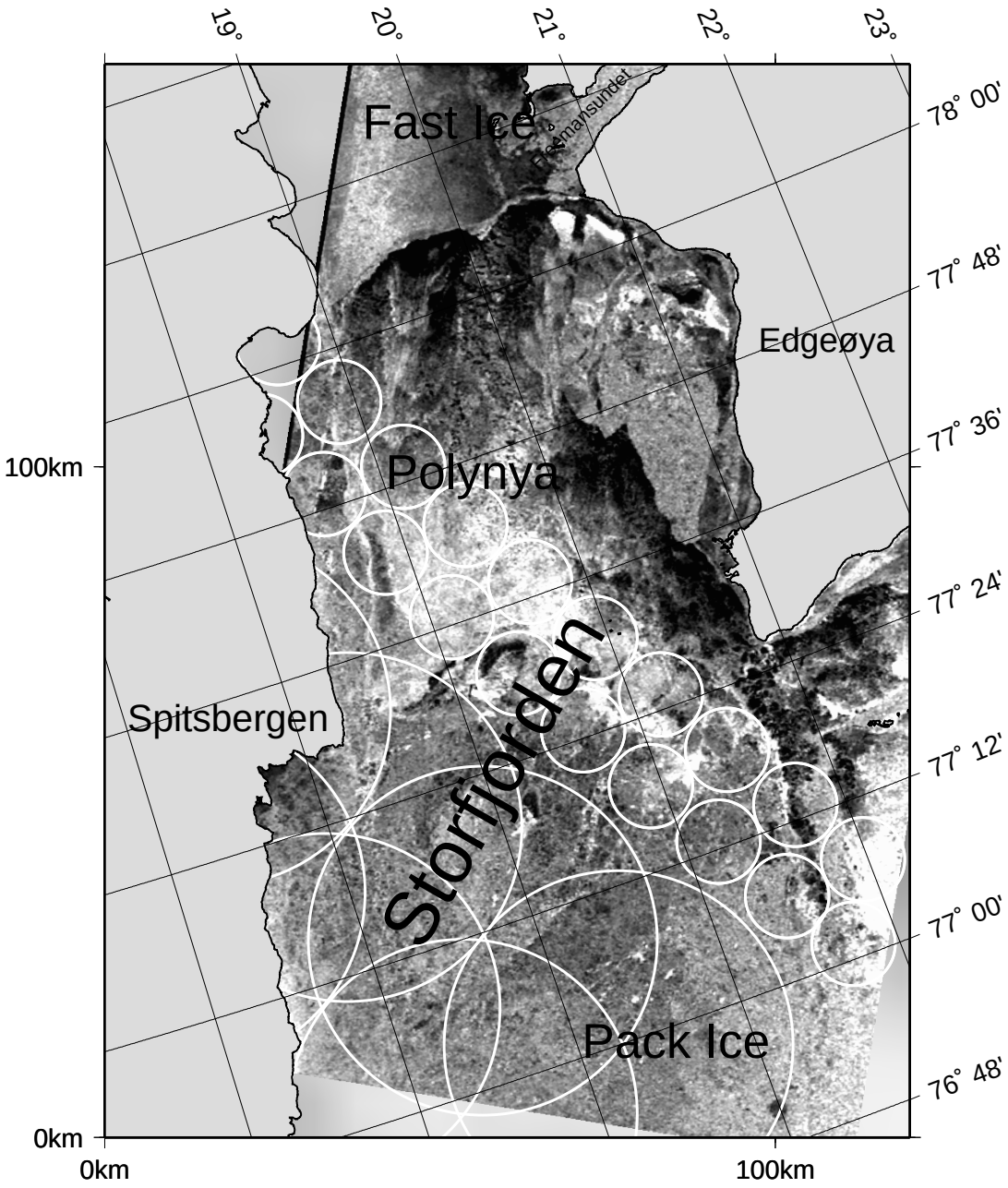

Figure 7: ERS-2 SAR image, April 9th, 1998. It shows the Storfjorden polynya, extending southward from the fast ice region in the north. The circles exemplify the different effective fields of view and sample distances of the SSM/I at 19 GHz (50 km circles) and 85 GHz (12 km circles). (Original ERS-SAR images (C)ESA 1998).

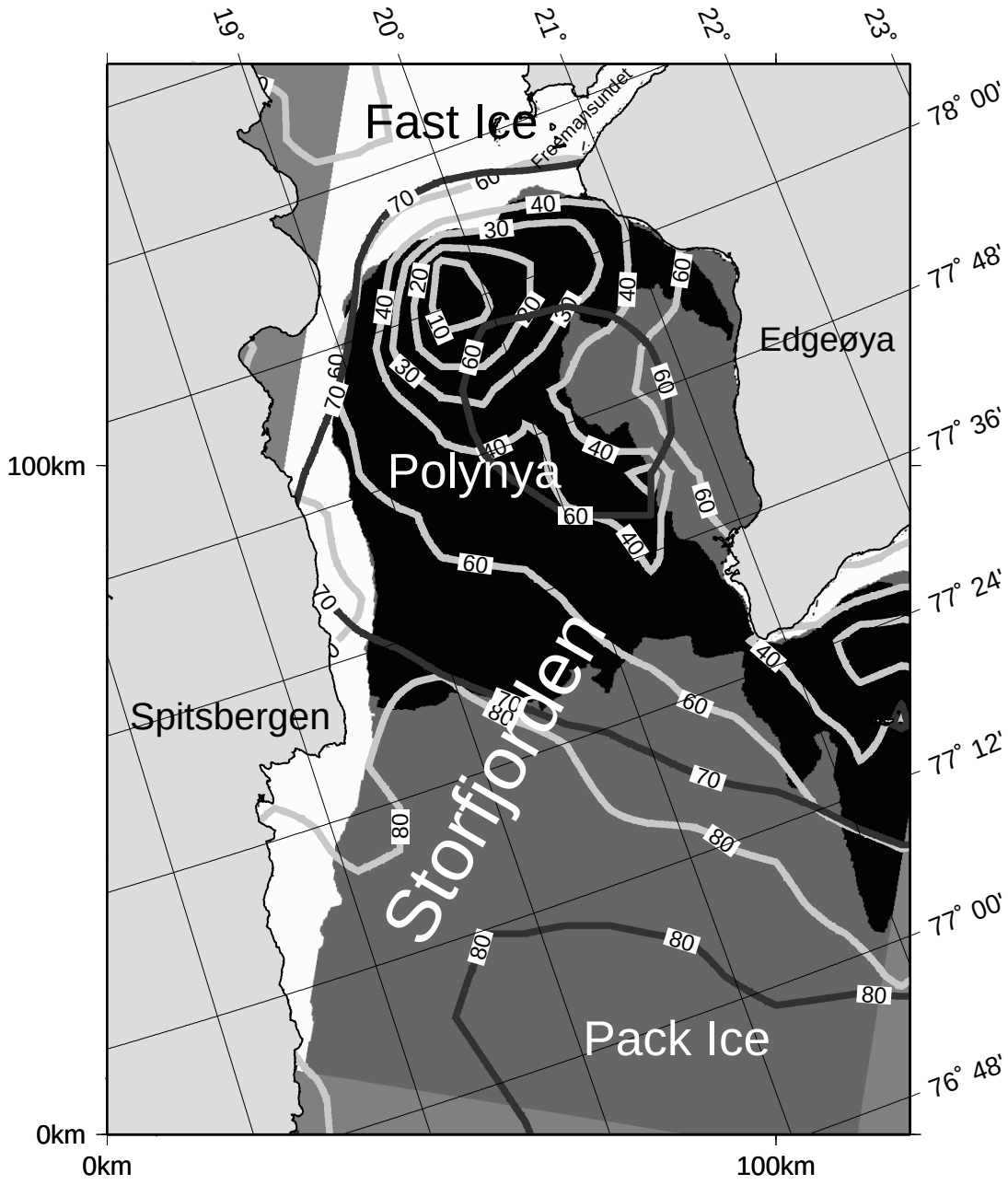

Figure 8: Segmented ERS-2 SAR image (white: fast ice, dark grey: pack ice, black: polynya), April 9th 1998. It is superimposed with isolines of the sea ice concentrations C(SSM/I; NTA) (dark grey) and C(SSM/I; ASI) (light grey).

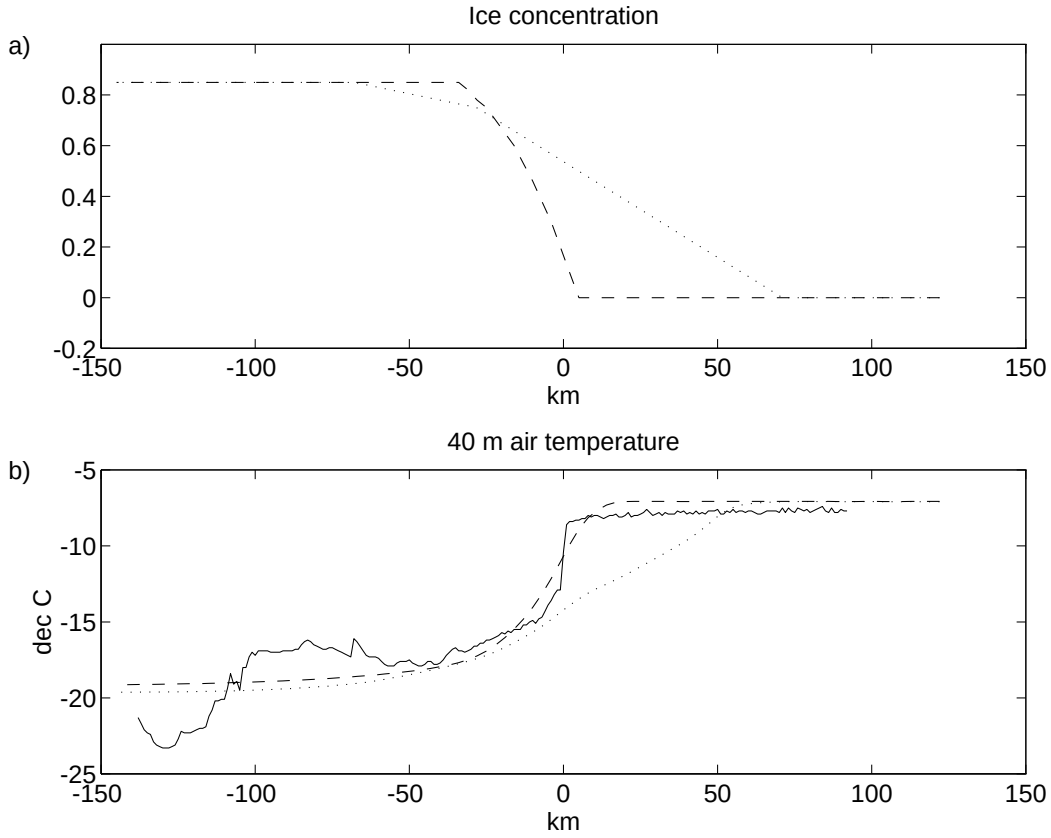

Figure 9: (a) Ice concentrations used in the model simulations based on the ASI algorithm (dashed) and NTA (dotted), (b) observed (solid) and modelled (ASI: dashed, NTA dotted) 40 m air temperatures over the ice edge zone in Storfjorden on March 30th, 1998.

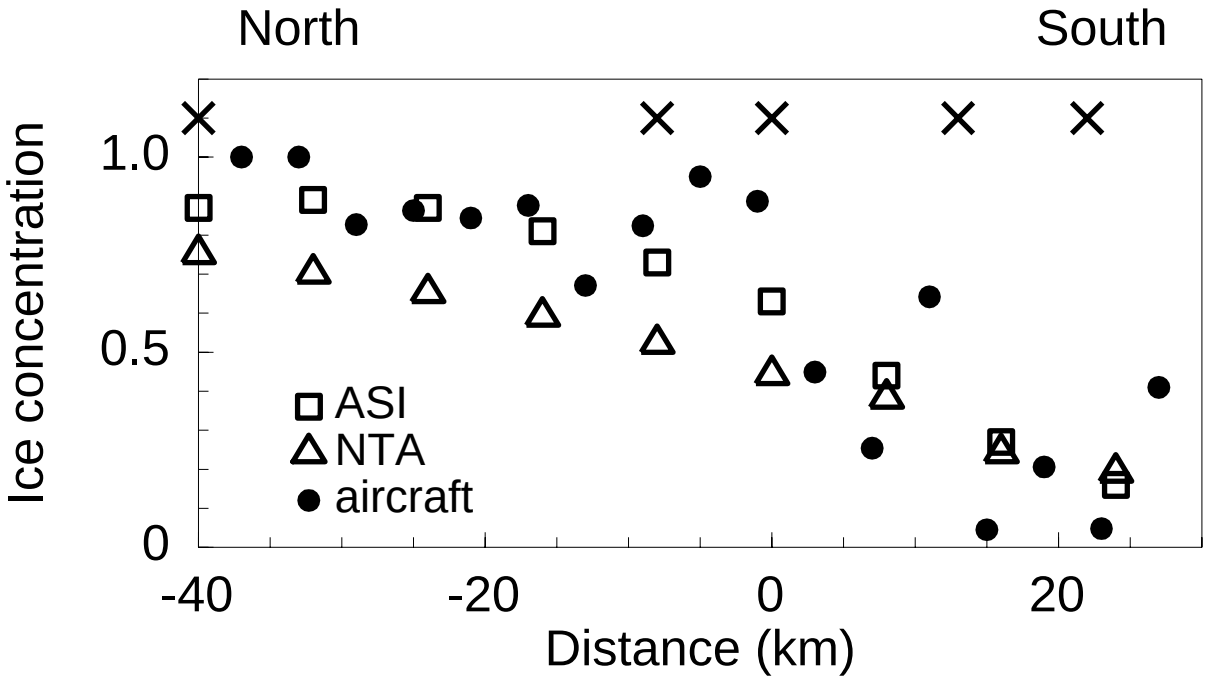

Figure 10: Ice concentration on April 5th, 1998 obtained with the two different algorithms. Crosses denote locations of aircraft observed temperature profiles (see Fig. 11).

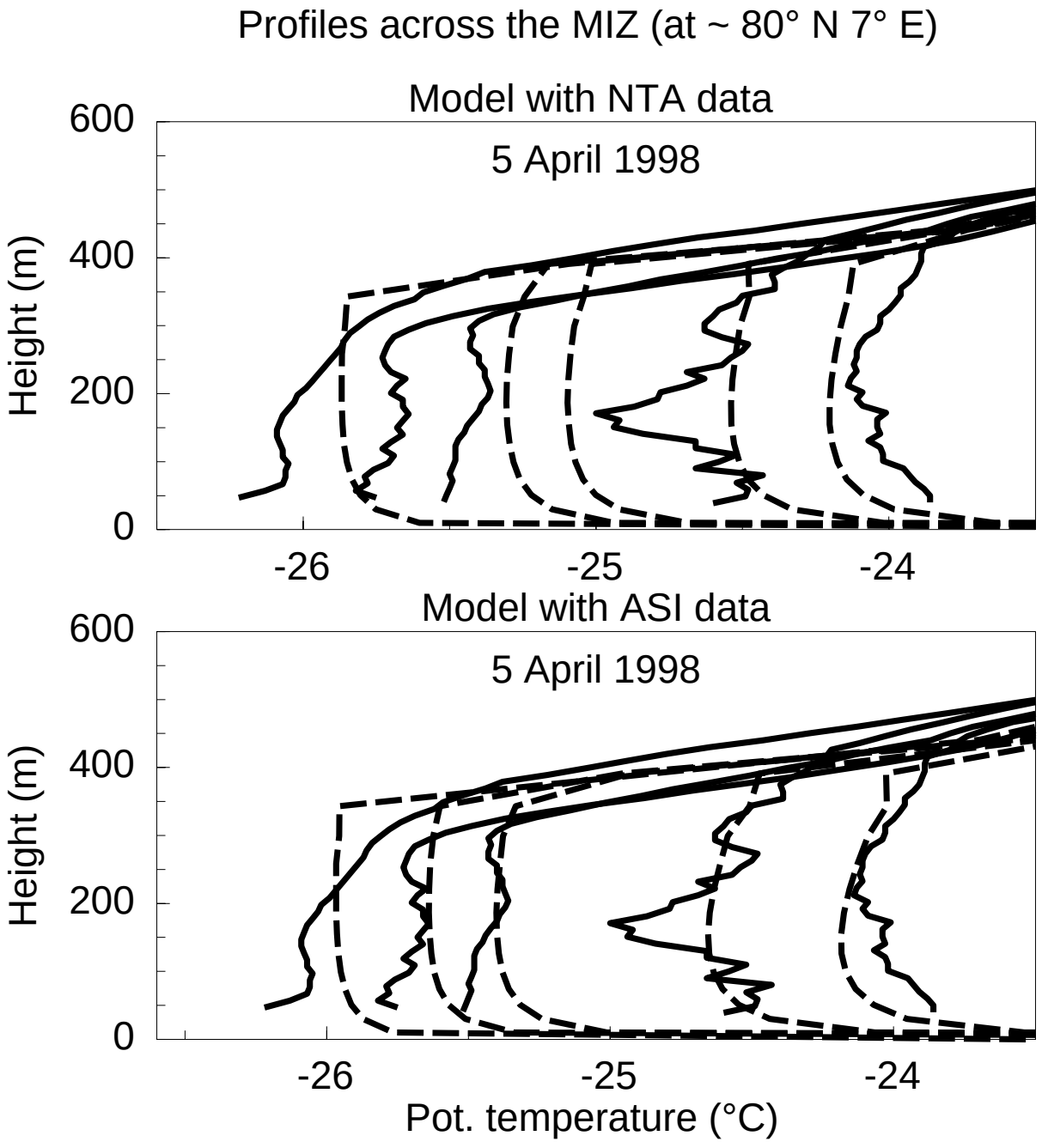

Figure 11: Observed (solid) and modeled (dashed) profiles of the potential temperature obtained from METRAS with ice concentration boundary conditions from different ice algorithms. Positions of profiles are marked with crosses in Figure 10, first profile on the left is at the northern end.